Supplementary Information for

Polymeric Nanocarrier *via* Metabolism Regulation Mediates Immunogenic Cell Death with Spatiotemporal Orchestration for Cancer Immunotherapy

Yichen Guo,[1,2,9] Yongjuan Li,[3,9] Mengzhe Zhang,[1,2] Rong Ma,[1,2] Yayun Wang,[1,2] Xiao Weng,[1,2] Jinjie Zhang,[1,2] Zhenzhong Zhang,[1,2]✉ Xiaoyuan Chen,[4,5,6,7,8]✉ and Weijing Yang[1,2]✉

[1] School of Pharmaceutical Sciences, Zhengzhou University, Zhengzhou 450001, China

[2] Henan Key Laboratory of Nanomedicine for Targeting Diagnosis and Treatment, Zhengzhou University, Zhengzhou 450001, Henan Province, China

[3] The Center of Infection and Immunity, Academy of Medical Sciences, Zhengzhou University, Zhengzhou, Henan 450001, China

[4] Departments of Diagnostic Radiology, Surgery, Chemical and Biomolecular Engineering, and Biomedical Engineering, Yong Loo Lin School of Medicine and College of Design and Engineering, National University of Singapore, Singapore, 119074, Singapore

[5] Clinical Imaging Research Centre, Centre for Translational Medicine, Yong Loo Lin School of Medicine, National University of Singapore, Singapore 117599, Singapore

[6] Nanomedicine Translational Research Program, Yong Loo Lin School of Medicine, National University of Singapore, Singapore 117597, Singapore

[7] Theranostics Center of Excellence (TCE), Yong Loo Lin School of Medicine, National University of Singapore, 11 Biopolis Way, Helios, Singapore 138667

[8] Institute of Molecular and Cell Biology, Agency for Science, Technology, and Research (A*STAR), 61 Biopolis Drive, Proteos, Singapore, 138673, Singapore

[9] These authors contributed equally: Yichen Guo and Yongjuan Li.

✉email: zhangzhenzhong@zzu.edu.cn (Z Zhang); chen.shawn@nus.edu.sg (X Chen); wjyang@zzu.edu.cn (W Yang)

Contents

Supplementary Figures

Supplementary Fig. 1. Synthesis of PEG-PMMA and PEG-PMMA-PDEA

Supplementary Fig. 2. Synthesis of monomer and copolymers.

Supplementary Fig. 3. ^{1}H NMR spectrum (400 MHZ, $CDCl_3$) of PEG-CPPA.

Supplementary Fig. 4. ^{1}H NMR spectrum (400 MHZ, $CDCl_3$) of PEG-PMMA.

Supplementary Fig. 5. ^{1}H NMR spectrum (400 MHZ, $CDCl_3$) of PEG-PMMA-PDEA.

Supplementary Fig. 6. ^{1}H NMR spectrum (400 MHZ, $CDCl_3$) of PPMA.

Supplementary Fig. 7. ^{1}H NMR spectrum (400 MHZ, $CDCl_3$) of PEG-PMMA-PPPMA.

Supplementary Fig. 8. ^{1}H NMR spectrum (400 MHZ, $CDCl_3$) of PEG-PMMA-P(PPMA-ME).

Supplementary Fig. 9. ^{1}H NMR spectrum (400 MHZ, $CDCl_3$) of PEG-PMMA-PPPMA.

Supplementary Fig. 10. ^{1}H NMR spectrum (400 MHZ, $CDCl_3$) of PEG-PMMA-P(PPMA-MPA).

Supplementary Fig. 11. ^{1}H NMR spectrum (400 MHZ, $CDCl_3$) of PEG-PMMA-P(PPMA-MPA-DEA).

Supplementary Fig. 12. pH responsiveness of nanocarriers determined by size changes in PBS buffer and acetate buffer at different time points.

Supplementary Fig. 13. Hydrodynamic size of $pRNC_{Thioether+DEA}$ and $pRNC_{DEA}$ in acetate buffer solution.

Supplementary Fig. 14. Scatter plots of the gating strategies for $CRT^{+}PI^{-}$ cells.

Supplementary Fig. 15. ICD inducibility of $pRNC_{Thiother+DEA}$ *via* detecting HMGB1 and ATP release.

Supplementary Fig. 16. ICD effect of $pRNC_{Thioether+DEA}$ on 4T1, MC38, LLC, Pan02 and U87-MG.

Supplementary Fig. 17. Colocalization of Cy5-$pRNC_{Thioether+DEA}$ with lysosome and Golgi apparatus in B16F10 cells characterized by CLSM.

Supplementary Fig. 18. ROS flow cytometry quantification.

Supplementary Fig. 19. Quantification of intracellular mtROS level.

Supplementary Fig. 20. Western blot of CHOP expression after different treatments.

Supplementary Fig. 21. Imaging of Calcein-AM (green channel, living cells) and PI (red channel, dead cells) staining of cells after different treatments.

Supplementary Fig. 22. Morphological features of cells after various treatments.

Supplementary Fig. 23. LDH activity in the supernatant after different treatments *via* microplate plate test kit characterization.

Supplementary Fig. 24. Representative flow cytometric images and the semi-quantitative analysis to show the apoptosis populations in B16F10 cells after different treatments.

Supplementary Fig. 25. $pRNC_{Thioether+DEA}$ mediated LPO generation.

Supplementary Fig. 26. LPO generation for B16F10 cells treated with different groups using C11-$BODIPY^{581/591}$ as a probe.

Supplementary Fig. 27. Western blot of MLKL expression in B16F10 cells after treatments with PBS, $pRNC_{Thioether+DEA}$ or $pRNC_{Thioether+DEA}$ + Nec-1s.

Supplementary Fig. 28. Representative flow cytometric images and the semi-quantitative analysis to show the cell death populations in B16F10 cells after treatment with PBS, $pRNC_{Thioether+DEA}$ with or without cell death inhibitors.

Supplementary Fig. 29. Synthesis of Man-PEG-PMMA-PPPMA and cRGD-PEG-PMMA-PPPMA.

Supplementary Fig. 30. ^1H NMR spectrum (400 MHZ, $CDCl_3$) of cRGD-PEG-PMMA-PPPMA.

Supplementary Fig. 31. ^1H NMR spectrum (400 MHZ, $CDCl_3$) of Man-PEG-PMMA-PPPMA.

Supplementary Fig. 32. Hydrodynamic size of cRGD-$pRNC_{Thioether+DEA}$@R848, Man-$pRNC_{Thioether+DEA}$ @R848, cRGD- *mix* Man-$pRNC_{Thioether+DEA}$, cRGD- *mix* Man-$pRNC_{Thioether+DEA}$@R848.

Supplementary Fig. 33. The standard curve of R848 is measured by fluorescence spectrophotometer.

Supplementary Fig. 34. *In vitro* R848 release from cRGD- *mix* Man-$pRNC_{Thioether+DEA}$ within 24 h at different pH values.

Supplementary Fig. 35. Dosage dependent cytotoxicity of $pRNC_{Thioether+DEA}$@FITC and cRGD-$pRNC_{Thioether+DEA}$@FITC in B16F10 cells by MTT assays.

Supplementary Fig. 36. Dosage dependent cytotoxicity of $pRNC_{Thioether+DEA}$@FITC and Man-$pRNC_{Thioether+DEA}$@FITC in RAW264.7 cells by MTT assays.

Supplementary Fig. 37. Cellular internalization of targeted nanoformulations *via* flow cytometry characterization.

Supplementary Fig. 38. Cellular internalization of different nanoformulations *via* CLSM characterization.

Supplementary Fig. 39. Representative flow cytometric images and quantification analysis of CRT exposure in B16F10 cells after different treatments via flow cytometry characterization.

Supplementary Fig. 40. Negative control of DC maturation investigation using viable B16F10 cells directly to incubate with DCs.

Supplementary Fig. 41. The ratio of DCs to dead cells after different treatments.

Supplementary Fig. 42. Representative immunofluorescence images showing tumor targeting of cRGD-$pRNC_{Thioether+DEA}$@DID.

Supplementary Fig. 43. Representative immunofluorescence images showing TAMs targeting of Man-pRNC$_{Thioether+DEA}$@FITC *in vivo*.
Supplementary Fig. 44. Flow cytometric analysis to show TAM polarization .
Supplementary Fig. 45. IL-12 and IL-10 levels in mice after different treatments.
Supplementary Fig. 46. Immune cell ratios analysis in tumor tissues.
Supplementary Fig. 47. Scatter plots show the gating strategies for $CD3^+CD8^+$ T cells.
Supplementary Fig. 48. Representative immunofluorescence images showing $CD3^+CD8^+$ T lymphocytes infiltration.
Supplementary Fig. 49. TNF-α level in mouse serum characterization by ELISA kit.
Supplementary Fig. 50. Representative immunofluorescence images of tumors with HMGB1 release.
Supplementary Fig. 51. Representative flow dot plots and statistics of CD8+Tetramer+ T cells in peripheral blood mononuclear cells of mice.
Supplementary Fig. 52. Quantitative ratio of $CD4^+$ in $CD3^+$ T cells.
Supplementary Fig. 53. Scatter plots of the gating strategies for $CD8^+PD\text{-}1^+$ T cells.
Supplementary Fig. 54. H&E staining of normal tissues harvested from mice in different groups.
Supplementary Fig. 55. H&E staining of normal tissues harvested from mice in different groups.

Supplementary Tables

Supplementary Table 1. Characteristics of block copolymers.
Supplementary Table 2. Preparation of blank polymersomes.
Supplementary Table 3. Drug loading content and efficiency characterization.

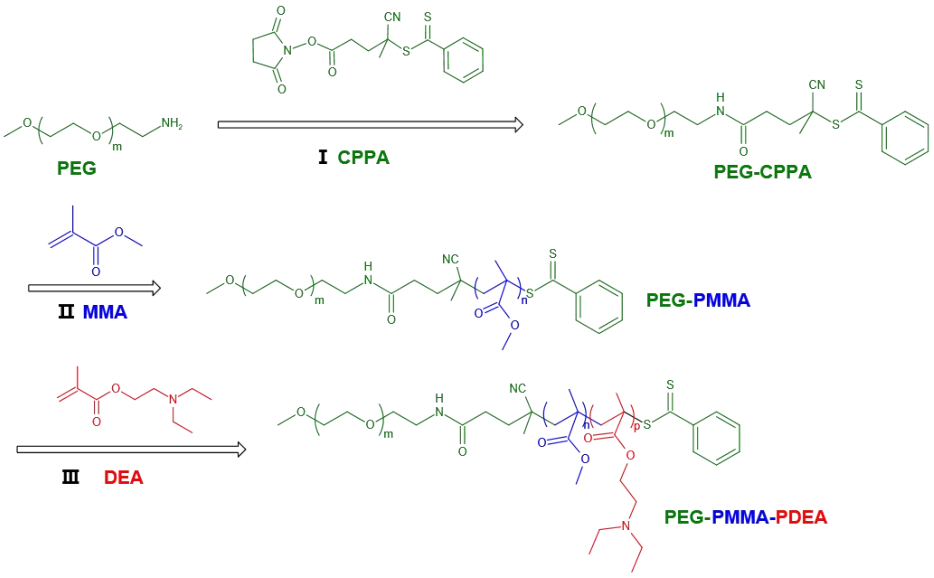

Supplementary Fig. 1. Synthesis of PEG-PMMA and PEG-PMMA-PDEA. Conditions: (I) TEA, DEA, 30 ℃, 24 h. (II) AIBN, 1,4-dioxane, 70 ℃, 48 h. (III) AIBN, 1,4-dioxane, 70 ℃, 48 h.

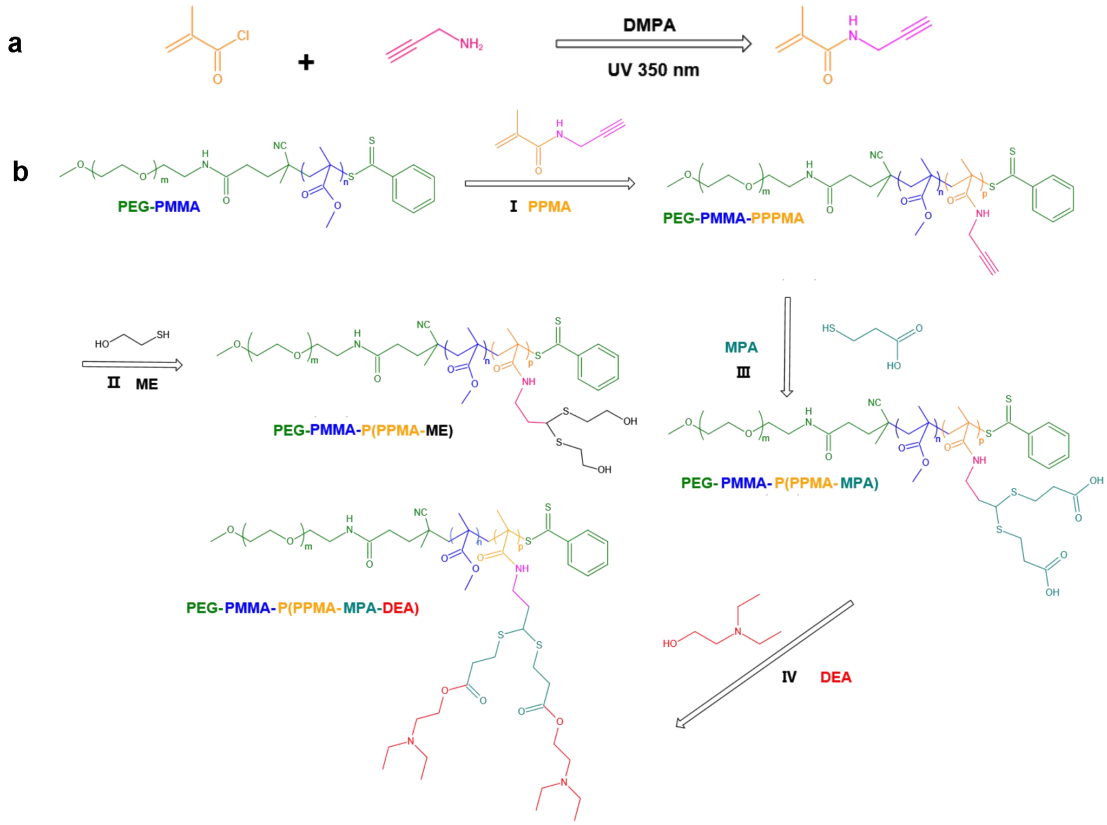

Supplementary Fig. 2. Synthesis of monomer and copolymers. a) Synthesis of PPMA. b) Synthesis of PEG-PMMA-PPPMA, PEG-PMMA-P(PPMA-ME), and PEG-PMMA-P(PPMA-MPA-DEA). Conditions: (I) AIBN, 1, 4-Dioxane, 70 ℃, 48 h. (II) DMPA, DMF, 30 ℃, 24 h. (III) DMPA, DMF, 30 ℃, 24 h. (IV) DMAP, EDC·HCl, DMF, 30 ℃, 24 h.

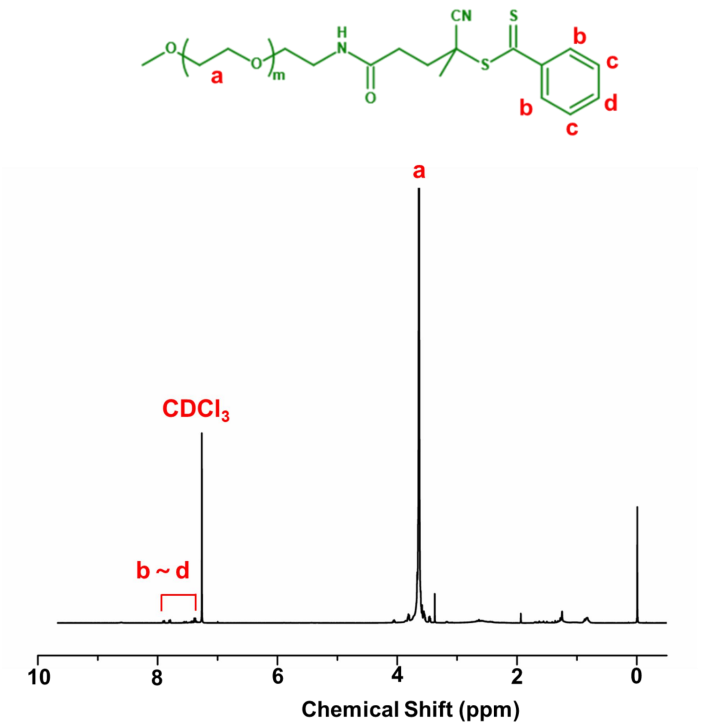

Supplementary Fig. 3. ^{1}H NMR spectrum (400 MHZ, $CDCl_3$) of PEG-CPPA.

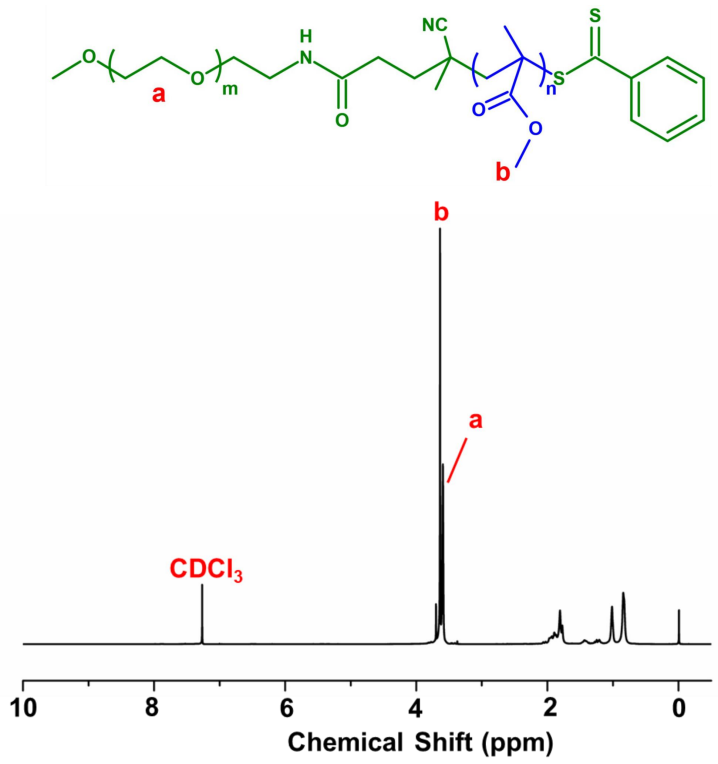

Supplementary Fig. 4. ^{1}H NMR spectrum (400 MHZ, $CDCl_3$) of PEG-PMMA.

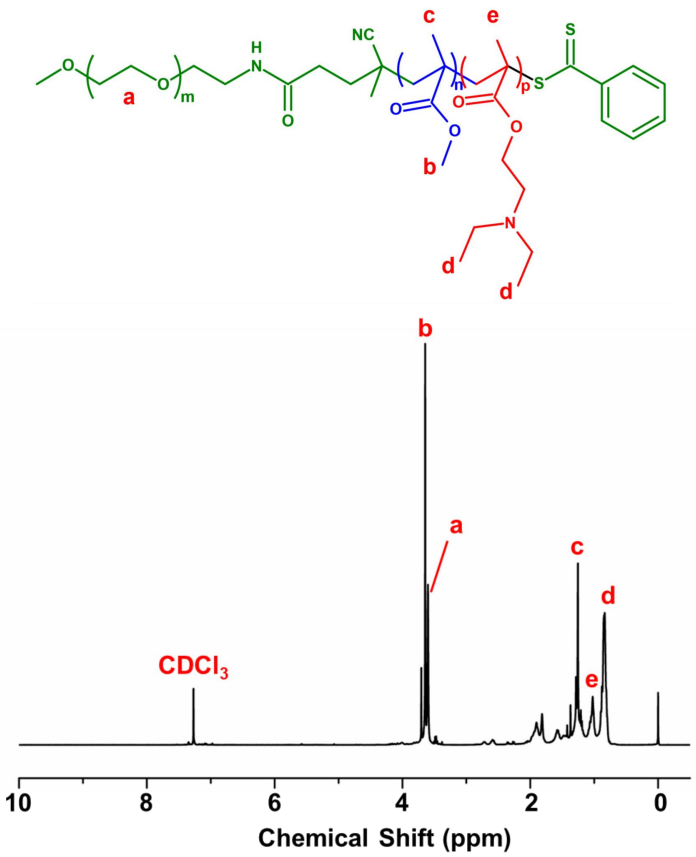

Supplementary Fig. 5. ^{1}H NMR spectrum (400 MHZ, $CDCl_3$) of PEG-PMMA-PDEA.

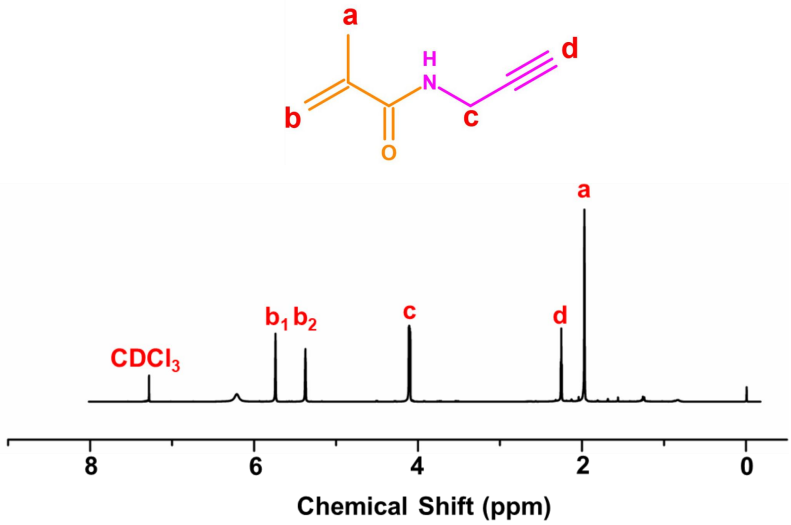

Supplementary Fig. 6. ^{1}H NMR spectrum (400 MHZ, $CDCl_3$) of PPMA.

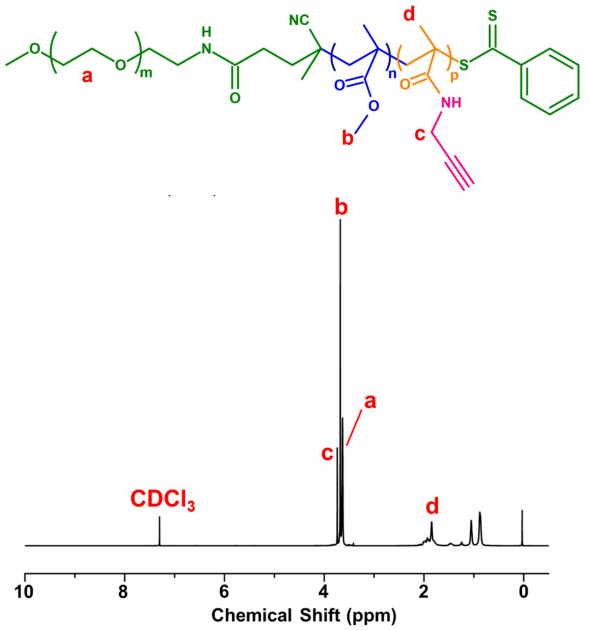

Supplementary Fig. 7. ^{1}H NMR spectrum (400 MHZ, $CDCl_3$) of PEG-PMMA-PPPMA with a molecular weight as 5.0-10.0-6.3 kg/mol.

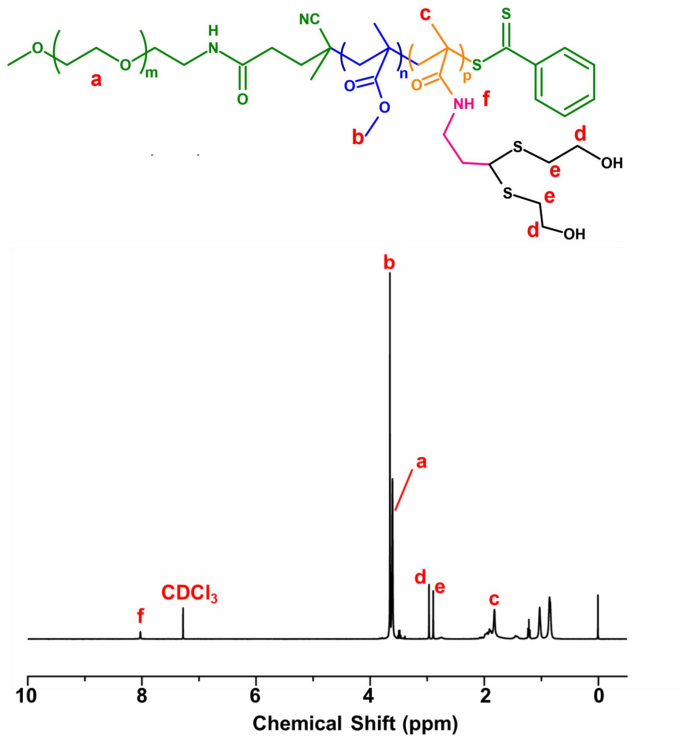

Supplementary Fig. 8. ^{1}H NMR spectrum (400 MHZ, $CDCl_3$) of PEG-PMMA-P(PPMA-ME).

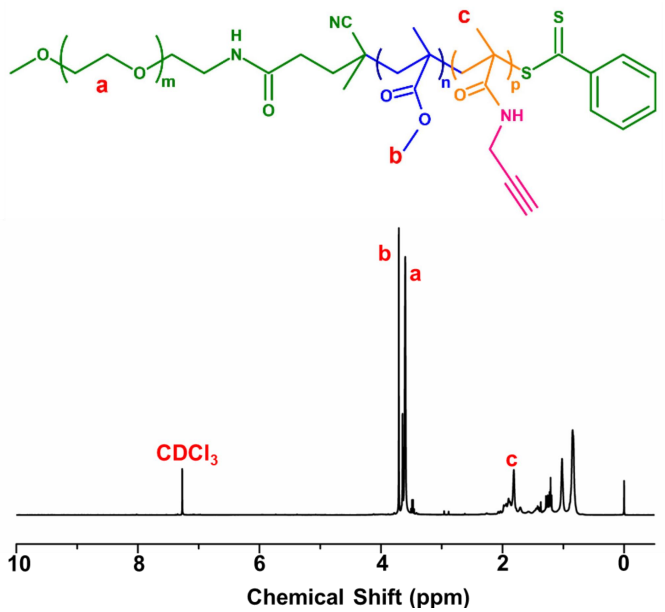

Supplementary Fig. 9. ^{1}H NMR spectrum (400 MHZ, $CDCl_3$) of PEG-PMMA-PPPMA with a molecular weight as 5.0-7.3-9.8 kg/mol.

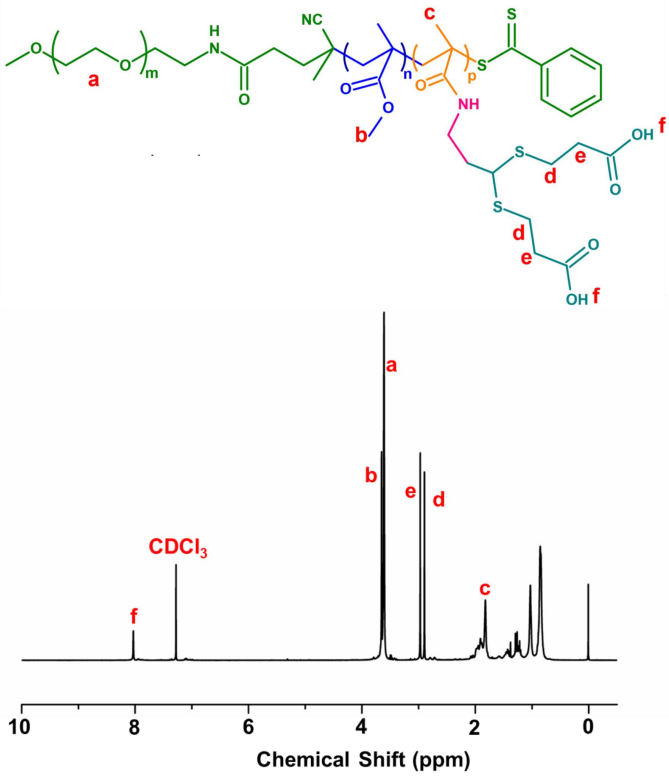

Supplementary Fig. 10. ^{1}H NMR spectrum (400 MHZ, $CDCl_3$) of PEG-PMMA-P(PPMA-MPA).

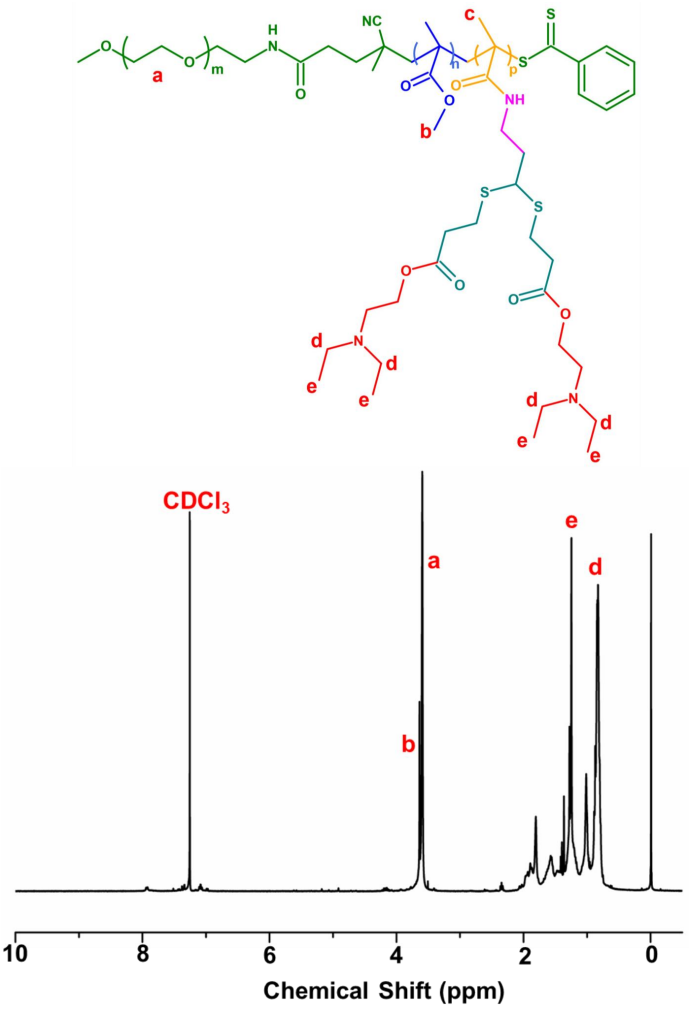

Supplementary Fig. 11. ^{1}H NMR spectrum (400 MHZ, $CDCl_3$) of PEG-PMMA-P(PPMA-MPA-DEA).

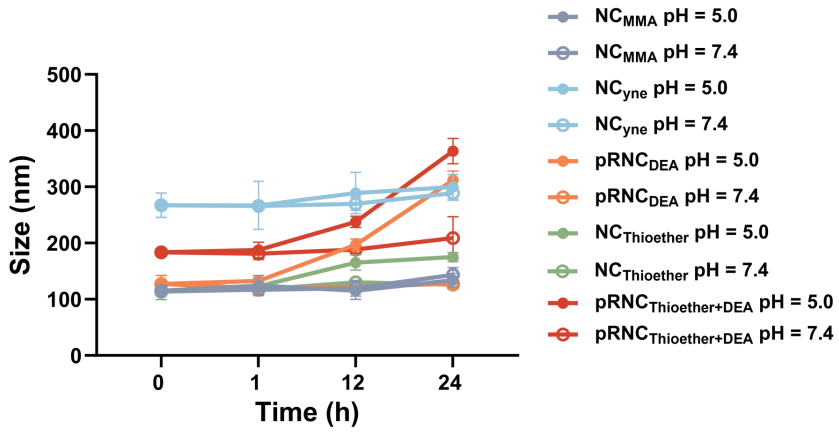

Supplementary Fig. 12. pH responsiveness of nanocarriers determined by size changes in PBS buffer (pH 7.4, 10 mM, 150 mM NaCl) and acetate buffer (pH 5.0, 10 mM, 150 mM NaCl) at different time points.

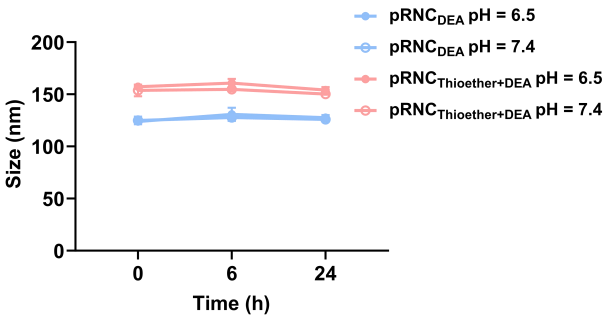

Supplementary Fig. 13. Hydrodynamic size of pRNC$_{Thioether+DEA}$ and pRNC$_{DEA}$ in acetate buffer solution (pH 6.5, 10 mM, 150 mM NaCl).

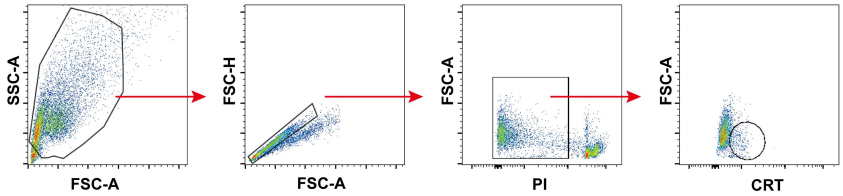

Supplementary Fig. 14. Scatter plots of the gating strategies for CRT^{+}PI^{-} cells.

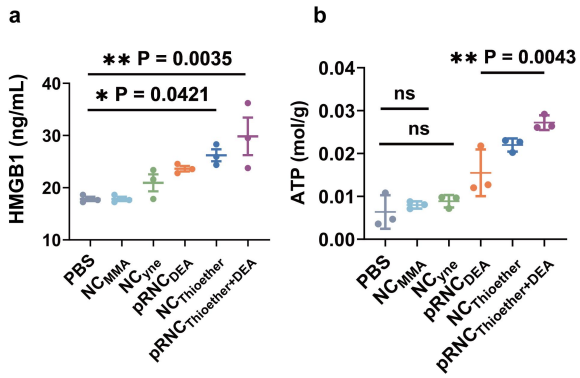

Supplementary Fig. 15. ICD inducibility of pRNC$_{Thiother+DEA}$ *via* detecting HMGB1 and ATP release. a) Release of HMGB1 in cell supernatant after different treatments *via* ELISA characterization (n = 3 independent experiments). b) ATP release after different treatments *via* ATP Assay Kit characterization (n = 3 independent experiments).

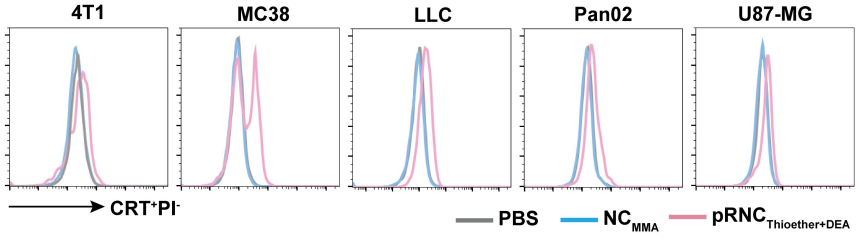

Supplementary Fig. 16. ICD effect of pRNC$_{Thioether+DEA}$ on 4T1, MC38, LLC, Pan02 and U87-MG after 48 h incubation, respectively.

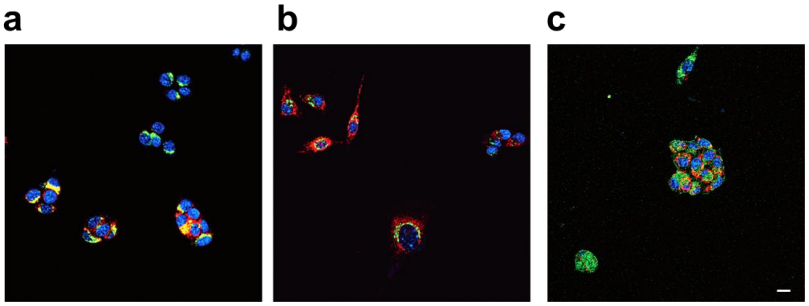

Supplementary Fig. 17. Colocalization of Cy5-pRNC$_{Thioether+DEA}$ with lysosome and Golgi apparatus in B16F10 cells characterized by CLSM. a, b) Representative images of Cy5-pRNC$_{Thioether+DEA}$ mediated lysosome colocalization at 2 and 4 h. Lysosome was stained with Lysosome Tracker green (green). c) Representative images of Cy5-pRNC$_{Thioether+DEA}$ mediated Golgi apparatus colocalization. Golgi was stained with Golgi-Tracker green (green). Red represented Cy5-pRNC$_{Thioether+DEA}$, and blue represented nuclei with DAPI staining. Scale bar = 20 μm.

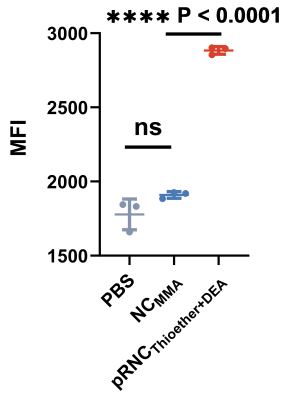

Supplementary Fig. 18. ROS flow cytometry quantification. Data are shown as mean ± SD (n = 3 independent experiments). The word "ns" represented non-significance, and $^{****}p < 0.0001$.

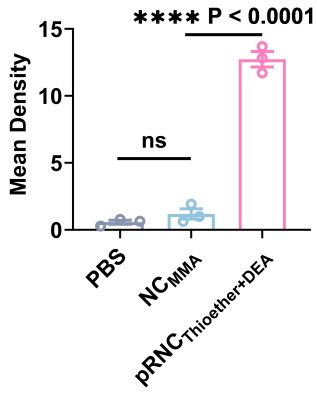

Supplementary Fig. 19. Quantification of intracellular mtROS level. Data are shown as

mean ± SEM (n = 3 independent experiments). The word "ns" represented non-significance, and $^{****}p < 0.0001$.

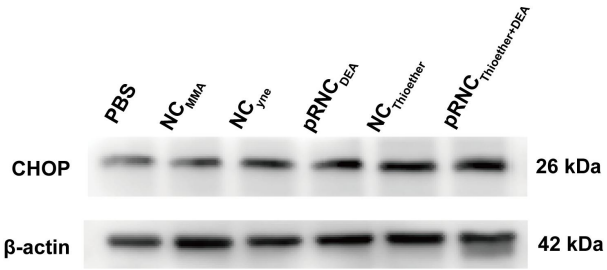

Supplementary Fig. 20. Western blot of CHOP expression after different treatments.

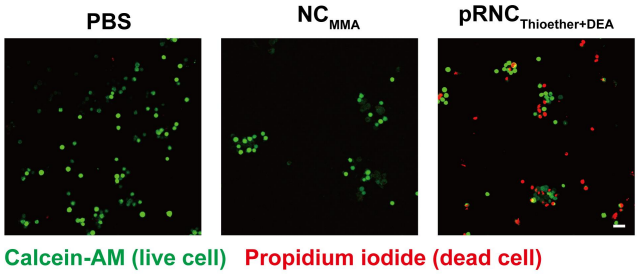

Supplementary Fig. 21. Imaging of Calcein-AM (green channel, living cells) and PI (red channel, dead cells) staining of cells after different treatments. Scale bar, 50 μm.

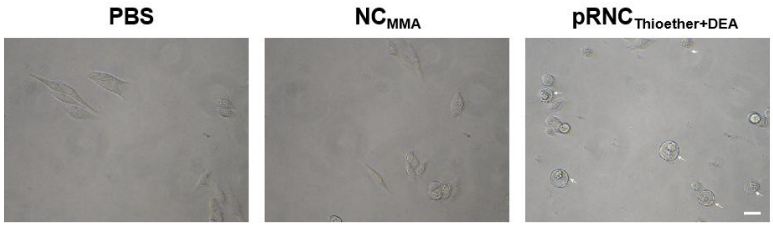

Supplementary Fig. 22. Morphological features of cells after various treatments. The white arrows represent pyroptotic cells. Scale bar, 30 μm.

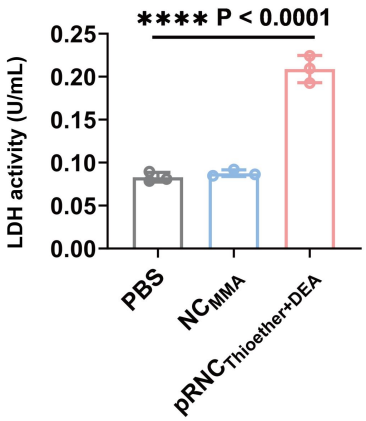

Supplementary Fig. 23. LDH activity in the supernatant after different treatments *via*

microplate plate test kit characterization (One unit means that pyruvate per micromole was produced in the reaction system when cell supernatant per milliliter was incubated with substrate at 37 °C for 15 min). Data are shown as mean ± SD (n = 3 independent experiments).

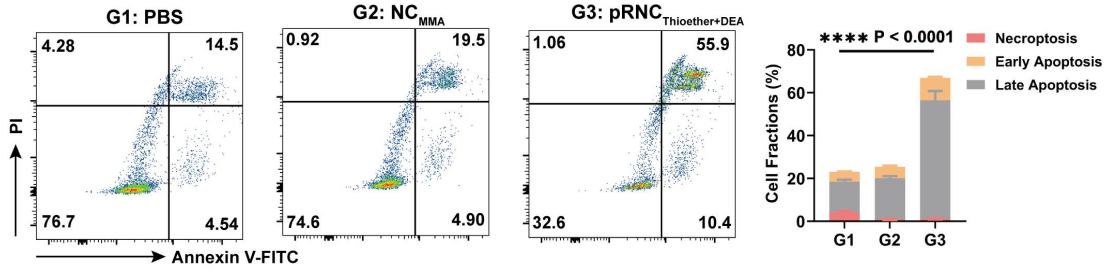

Supplementary Fig. 24. Representative flow cytometric images and the semi-quantitative analysis to show the apoptosis populations in B16F10 cells after different treatments. Data are shown as mean ± SD (n = 3 independent experiments), $^{****}P < 0.0001$.

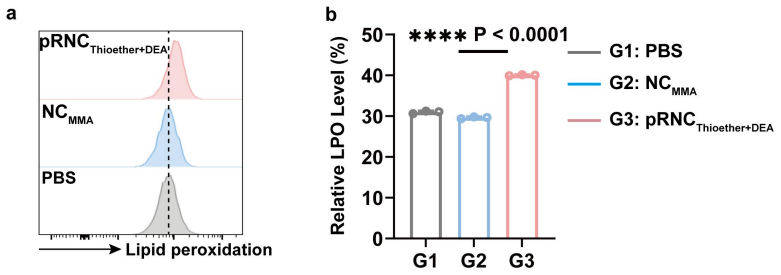

Supplementary Fig. 25. pRNC$_{Thioether+DEA}$ mediated LPO generation. a) Representative flow cytometric image and b) the semi-quantitative analysis of flow cytometric to show the LPO generation for B16F10 cells treated with different groups using C11-BODIPY581/591. Data are shown as mean ± SD, n = 3 independent experiments, $^{****}P < 0.0001$.

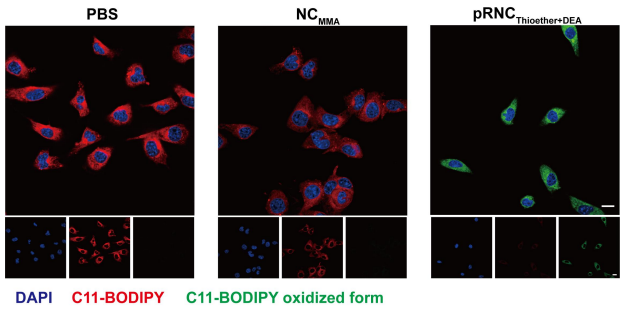

Supplementary Fig. 26. LPO generation for B16F10 cells treated with different groups using C11-BODIPY$^{581/591}$ as a probe. Scale bar, 20 μm.

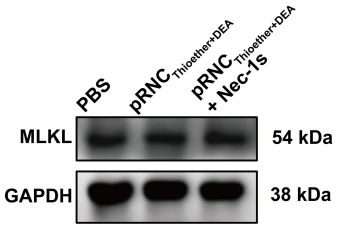

Supplementary Fig. 27. Western blot of MLKL expression in B16F10 cells after treatments with PBS, $pRNC_{Thioether+DEA}$ or $pRNC_{Thioether+DEA}$ + Nec-1s. GADPH was used as internal control.

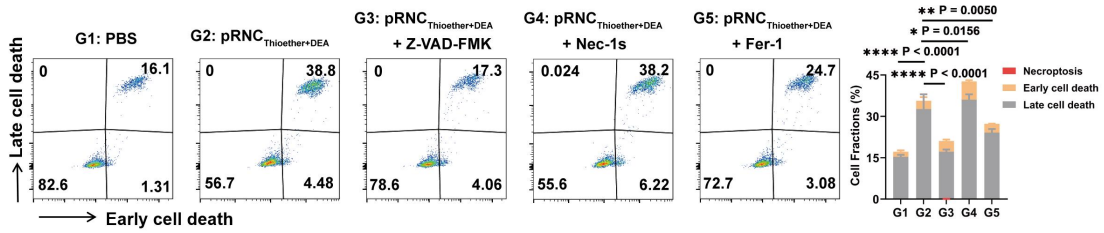

Supplementary Fig. 28. Representative flow cytometric images and the semi-quantitative analysis to show the cell death populations in B16F10 cells after treatment with PBS, $pRNC_{Thioether+DEA}$ with or without cell death inhibitors. Data are shown as mean ± SD (n = 3 independent experiments), $^{*}P < 0.05$, $^{**}P < 0.01$, $^{***}P < 0.001$, and $^{****}P < 0.0001$.

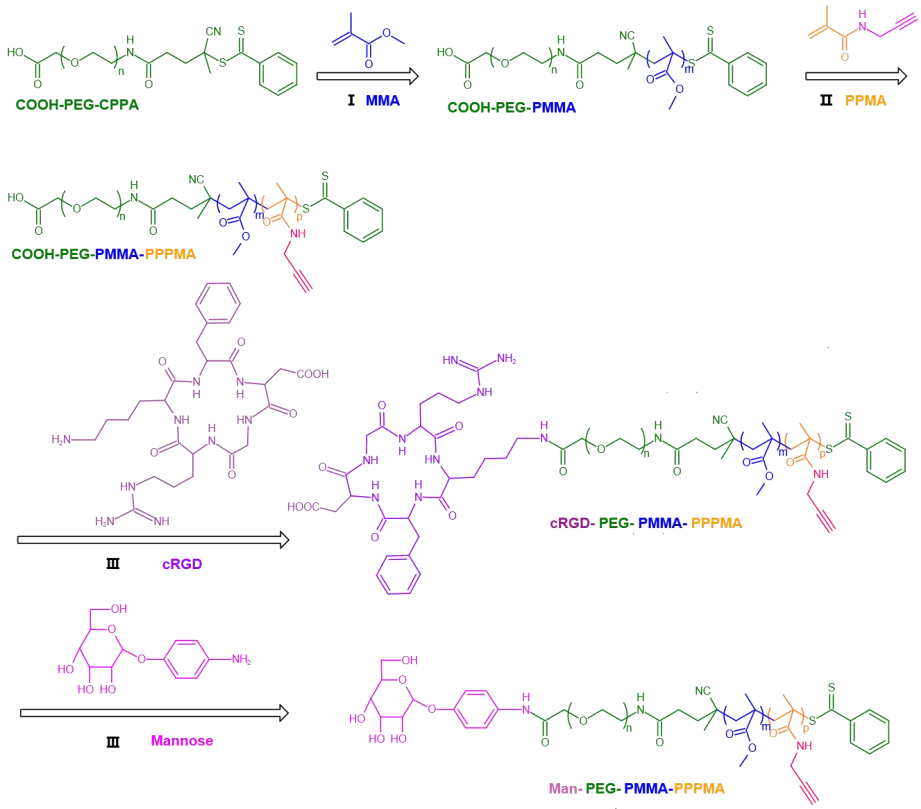

Supplementary Fig. 29. Synthesis of Man-PEG-PMMA-PPPMA and cRGD-PEG-PMMA-

PPPMA. Conditions: (I) AIBN, 1, 4-dioxane, 70 ℃, 48 h. (II) AIBN, 1, 4-dioxane, 70 ℃, 48 h. (III) EDC·HCl, NHS, DMF, 30 ℃, 24 h.

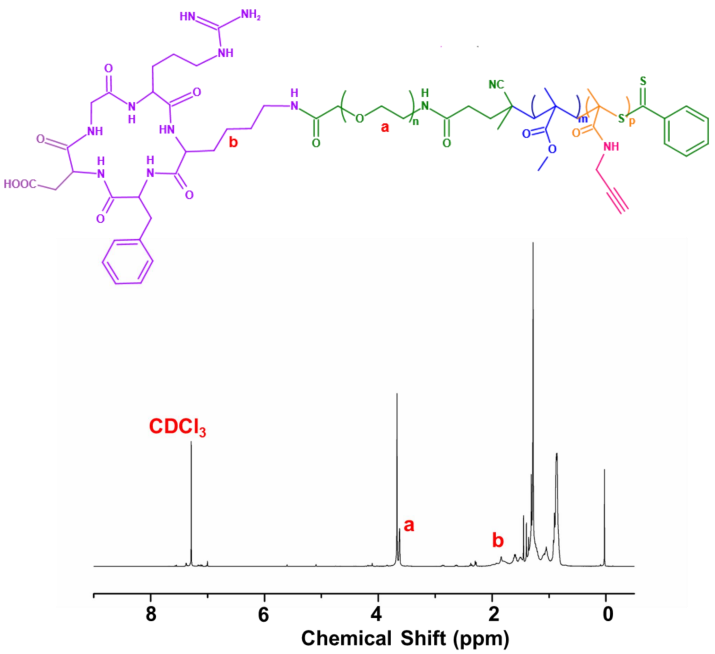

Supplementary Fig. 30. ^{1}H NMR spectrum (400 MHZ, $CDCl_3$) of cRGD-PEG-PMMA-PPPMA.

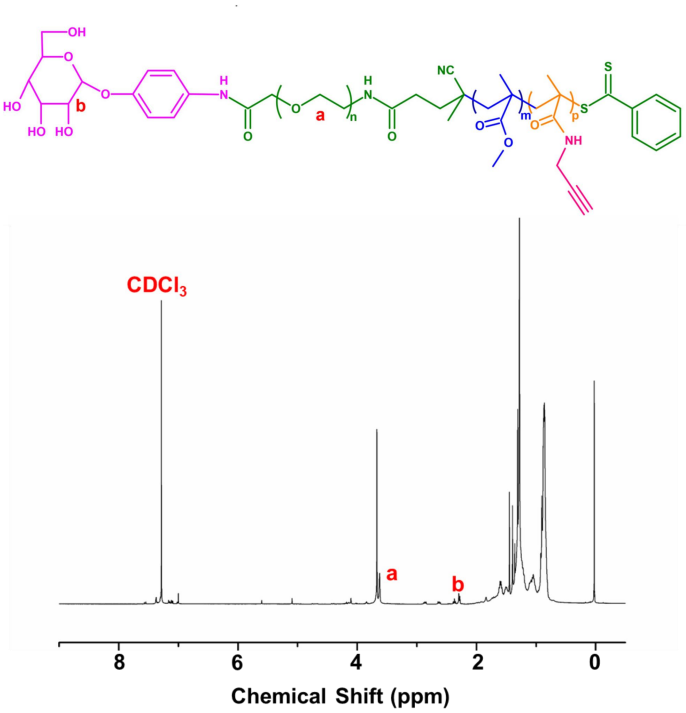

Supplementary Fig. 31. ^{1}H NMR spectrum (400 MHZ, $CDCl_3$) of Man-PEG-PMMA-PPPMA.

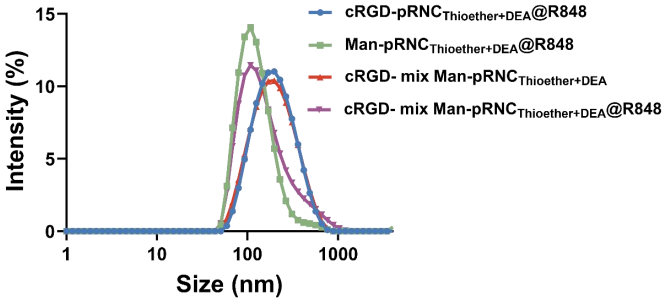

Supplementary Fig. 32. Hydrodynamic size of cRGD-pRNC$_{Thioether+DEA}$@R848, Man-pRNC$_{Thioether+DEA}$@R848, cRGD- *mix* Man-pRNC$_{Thioether+DEA}$, cRGD- *mix* Man-pRNC$_{Thioether+DEA}$@R848.

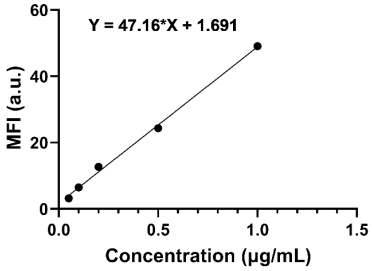

Supplementary Fig. 33. The standard curve of R848 is measured by fluorescence spectrophotometer.

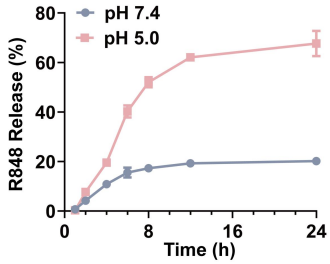

Supplementary Fig. 34. *In vitro* R848 release from cRGD- *mix* Man-pRNC$_{Thioether+DEA}$ within 24 h at different pH values (pH 7.4 or 5.0) (n = 3 independent experiments).

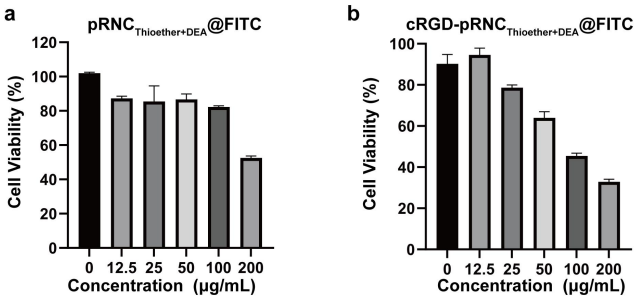

Supplementary Fig. 35. Dosage dependent cytotoxicity of a) pRNC$_{Thioether+DEA}$@FITC and b) cRGD-pRNC$_{Thioether+DEA}$@FITC in B16F10 cells by MTT assays. Data are shown as mean ± SD (n = 4 independent experiments).

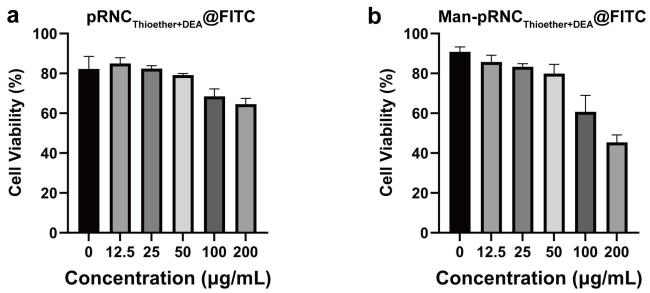

Supplementary Fig. 36. Dosage dependent cytotoxicity of a) $pRNC_{Thioether+DEA}$@FITC and b) Man-$pRNC_{Thioether+DEA}$@FITC in RAW264.7 cells by MTT assays. Data are shown as mean ± SD (n = 4 independent experiments).

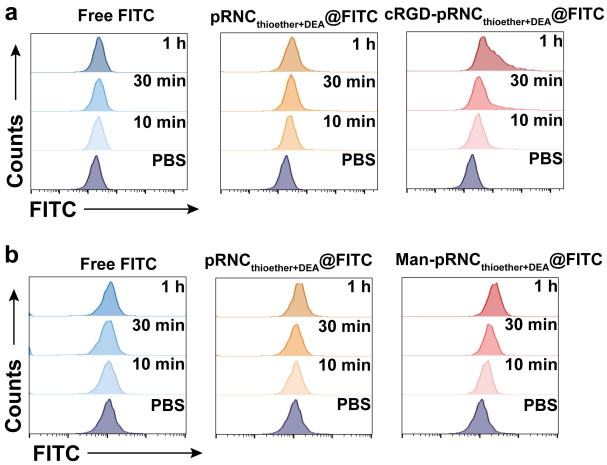

Supplementary Fig. 37. Cellular internalization of targeted nanoformulations *via* flow cytometry characterization. Representative flow cytometric plots showing the cellular uptake of a) $pRNC_{Thioether+DEA}$, cRGD-$pRNC_{Thioether+DEA}$ and free FITC at different time points in B16F10 cells and b) $pRNC_{Thioether+DEA}$, Man-$pRNC_{Thioether+DEA}$ and free FITC in RAW 264.7 cells.

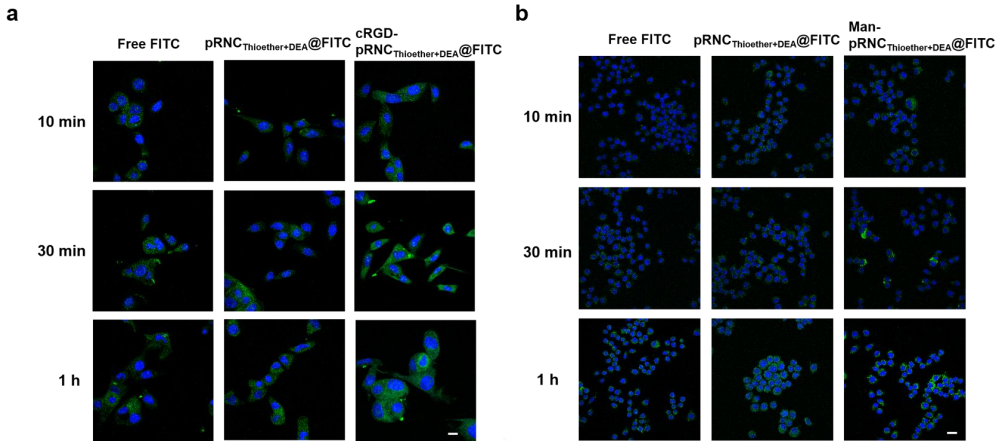

Supplementary Fig. 38. Cellular internalization of different nanoformulations *via* CLSM characterization. Representative images of a) cRGD-$pRNC_{Thioether+DEA}$@FITC uptake in

B16F10 cells, and b) Man-pRNC$_{Thioether+DEA}$@FITC in RAW264.7 cells. Scale bar = 20 μm.

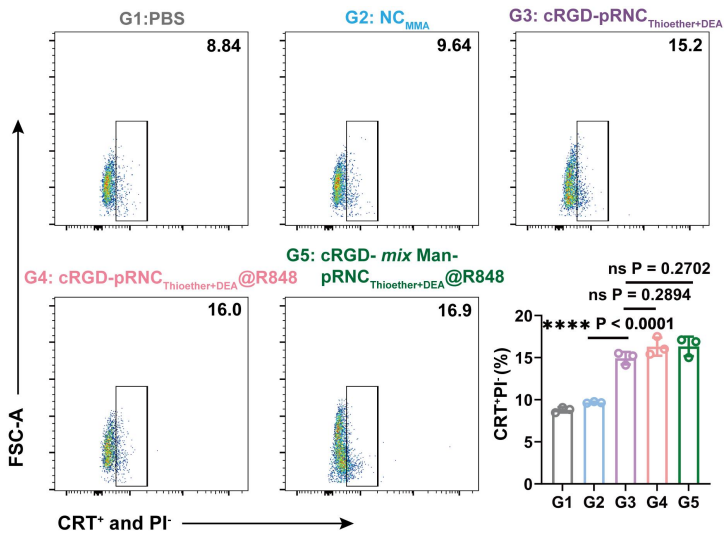

Supplementary Fig. 39. Representative flow cytometric images and quantification analysis of CRT exposure in B16F10 cells after different treatments *via* flow cytometry characterization. Data are presented as mean ± SD (n = 3 independent experiments). Statistical significance was calculated through one-way ANOVA for multiple comparisons using a Tukey post-hoc test.

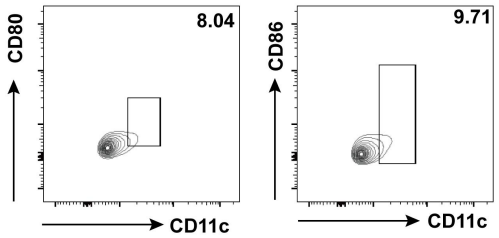

Supplementary Fig. 40. Negative control of DC maturation investigation using viable B16F10 cells directly to incubate with DCs.

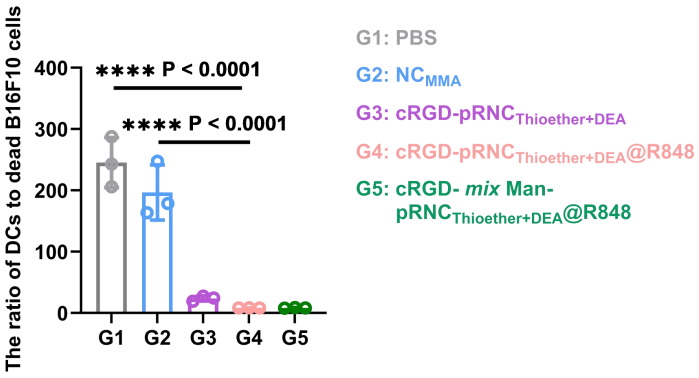

Supplementary Fig. 41. The ratio of DCs to dead B16F10 cells after different treatments. Data are presented as mean ± SD (n = 3 independent experiments). Statistical significance was

calculated through one-way ANOVA for multiple comparisons using a Tukey post-hoc test.

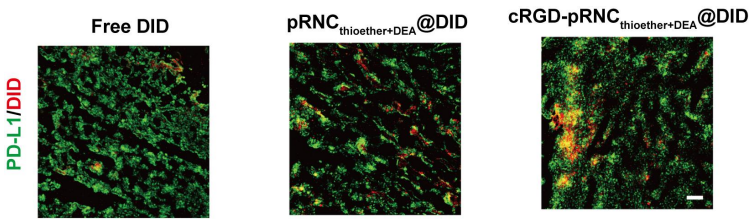

Supplementary Fig. 42. Representative immunofluorescence images showing tumor targeting of cRGD-pRNC$_{\text{Thioether+DEA}}$@DID at 24 h treatment. Scale bar = 50 μm.

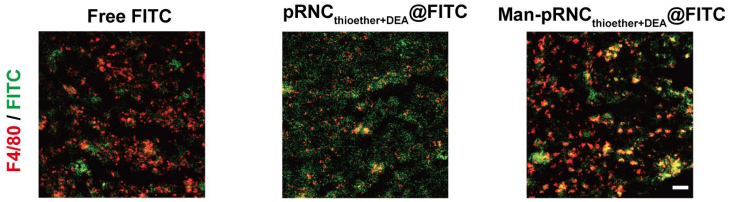

Supplementary Fig. 43. Representative immunofluorescence images showing TAMs targeting of Man-pRNC$_{\text{Thioether+DEA}}$@FITC *in vivo* at 24 h treatment. Scale bar = 50 μm.

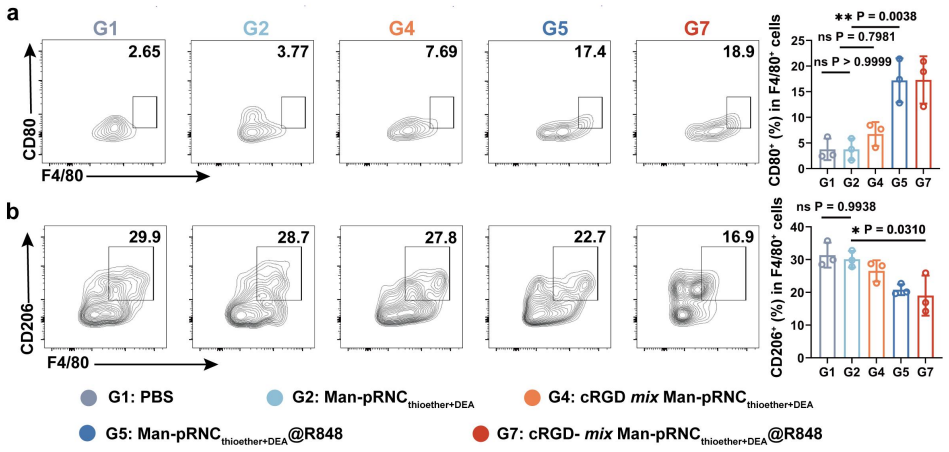

Supplementary Fig. 44. Flow cytometric analysis to show TAM polarization. a) Representative flow cytometry plots (left) and quantitative analysis (right) of $CD80^{+}F4/80^{+}$ TAM. b) Representative flow cytometry images (left) and quantitative data (right) of $CD206^{+}F4/80^{+}$ TAM. Data are presented as mean ± SD (n = 3 mice per group). Statistical significance was calculated through one-way ANOVA for multiple comparisons using a Tukey post-hoc test.

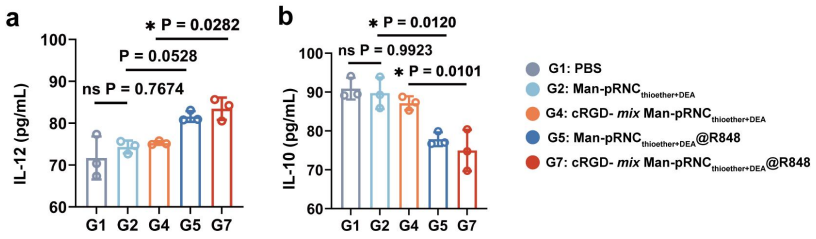

Supplementary Fig. 45. IL-12 and IL-10 levels in mice after different treatments. a) IL-12 and b) IL-10 levels measured by ELISA. Data are presented as mean ± SD (n = 3 mice per group). Statistical significance was calculated through one-way ANOVA for multiple comparisons using a Tukey post-hoc test.

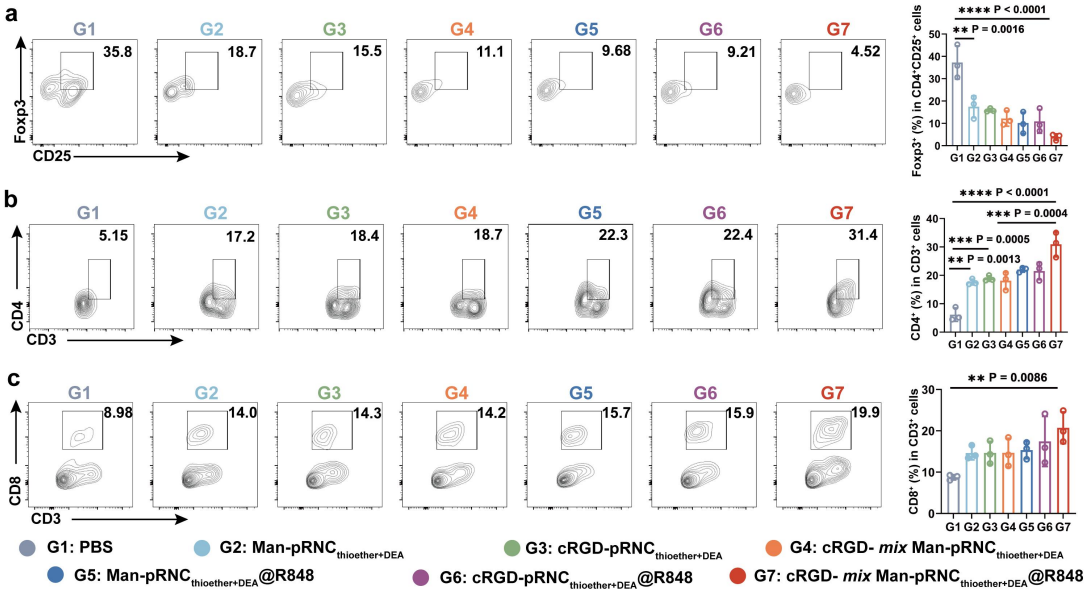

Supplementary Fig. 46. Immune cell ratios analysis in tumor tissues for mice after different treatments. a) Representative flow cytometric analysis gating on $CD25^+$ cells and quantification of $Foxp3^+$ Tregs in tumors. b) Representative flow cytometric analysis and quantification of $CD4^+$ gating on $CD3^+$ T cells. c) Representative flow cytometric analysis and quantification of $CD8^+$ gating on $CD3^+$ T cells. Data are presented as mean ± SD (n = 3 mice per group). Statistical significance was calculated through one-way ANOVA for multiple comparisons using a Tukey post-hoc test.

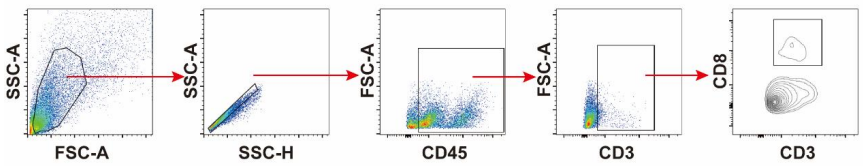

Supplementary Fig. 47. Scatter plots show the gating strategies for $CD3^+CD8^+$ T cells.

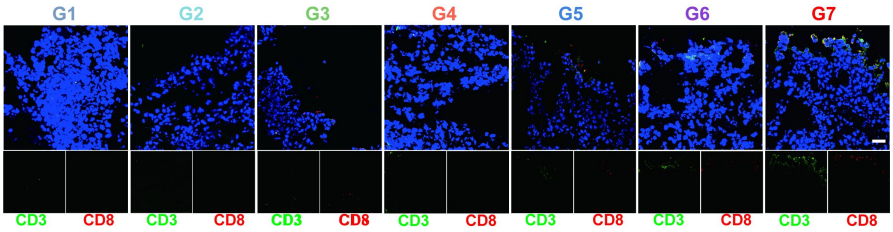

Supplementary Fig. 48. Representative immunofluorescence images showing $CD3^{+}CD8^{+}$ T lymphocytes infiltration. Nuclei were stained with DAPI. Scale bar = 50 μm. (G1: PBS, G2: Man-$pRNC_{Thioether+DEA}$, G3: cRGD-$PRNC_{Thiorther+DEA}$, G4: cRGD- *mix* Man-$pRNC_{Thioether+DEA}$, G5: Man-$pRNC_{Thioether+DEA}$@R848, G6: cRGD-$PRNC_{Thiorther+DEA}$@R848, G7: cRGD- *mix* Man- $pRNC_{Thioether+DEA}$@R848)

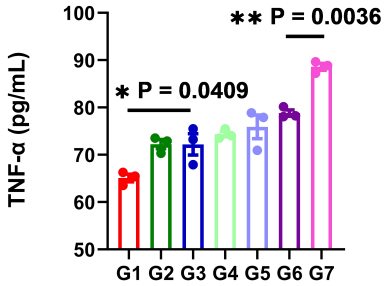

Supplementary Fig. 49. TNF-α level in mouse serum characterization by ELISA kit. (G1: PBS, G2: Man-$pRNC_{Thioether+DEA}$, G3: cRGD-$PRNC_{Thiorther+DEA}$, G4: cRGD- *mix* Man-$pRNC_{Thioether+DEA}$, G5: Man-$pRNC_{Thioether+DEA}$@R848, G6: cRGD-$PRNC_{Thiorther+DEA}$@R848, G7: cRGD- *mix* Man- $pRNC_{Thioether+DEA}$@R848). Data are presented as mean ± SEM (n = 3 mice per group). Statistical significance was calculated through one-way ANOVA for multiple comparisons using a Tukey post-hoc test.

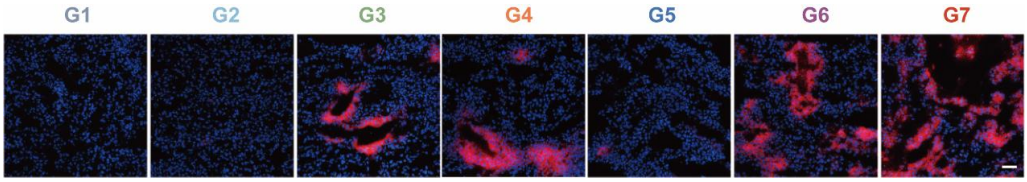

Supplementary Fig. 50. Representative immunofluorescence images of tumors with HMGB1 release. Red represented HMGB1 stained with Alexa Fluor®647 anti HMGB1, and blue represented nuclei stained with DAPI. Scale bar = 50 μm. (G1: PBS, G2: Man-$pRNC_{Thioether+DEA}$, G3: cRGD-$PRNC_{Thiorther+DEA}$, G4: cRGD- *mix* Man-$pRNC_{Thioether+DEA}$, G5: Man-$pRNC_{Thioether+DEA}$@R848, G6: cRGD-$PRNC_{Thiorther+DEA}$@R848, G7: cRGD- *mix* Man-$pRNC_{Thioether+DEA}$@R848).

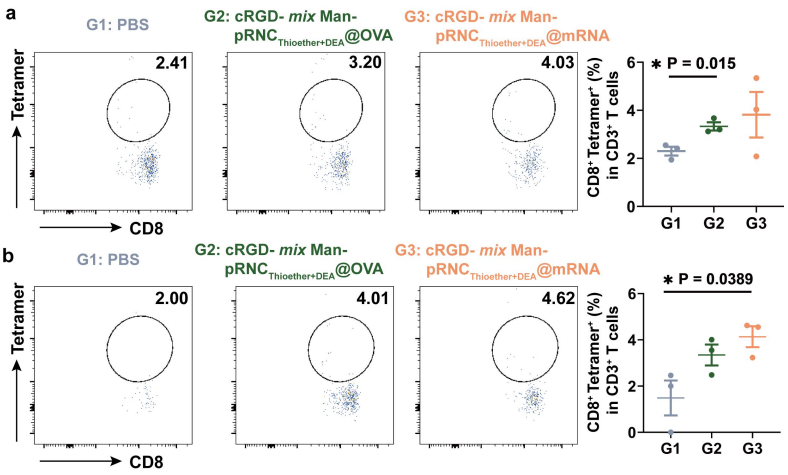

Supplementary Fig. 51. Representative flow dot plots and statistics of $CD8^+Tetramer^+$ T cells in peripheral blood mononuclear cells of mice a) day-7 and b) day-14 after immunization. Data are presented as mean ± SEM (n = 3 mice per group). Statistical significance was calculated through two-tailed student's *t* test.

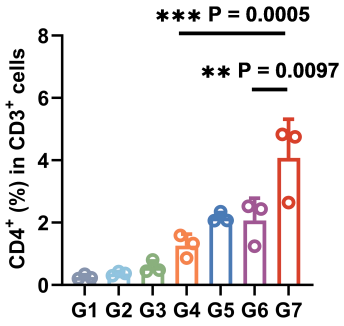

Supplementary Fig. 52. Quantitative ratio of $CD4^+$ in $CD3^+$ T cells. (G1: PBS, G2: Man-$pRNC_{Thioether+DEA}$, G3: cRGD-$PRNC_{Thiorther+DEA}$, G4: cRGD- *mix* Man-$pRNC_{Thioether+DEA}$, G5: Man-$pRNC_{Thioether+DEA}$@R848, G6: cRGD-$PRNC_{Thiorther+DEA}$@R848, G7: cRGD- *mix* Man-$pRNC_{Thioether+DEA}$@R848). Data are presented as mean ± SD (n = 3 mice per group). Statistical significance was calculated through one-way ANOVA for multiple comparisons using a Tukey post-hoc test.

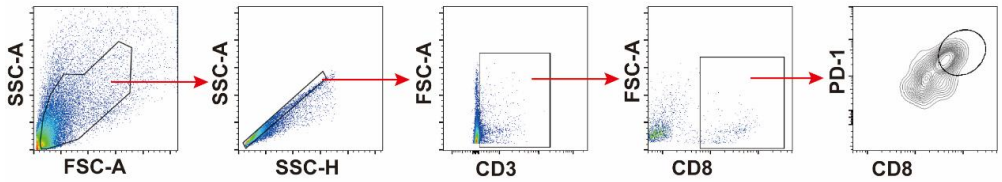

Supplementary Fig. 53. Scatter plots of the gating strategies for $CD8^+PD\text{-}1^+$ T cells.

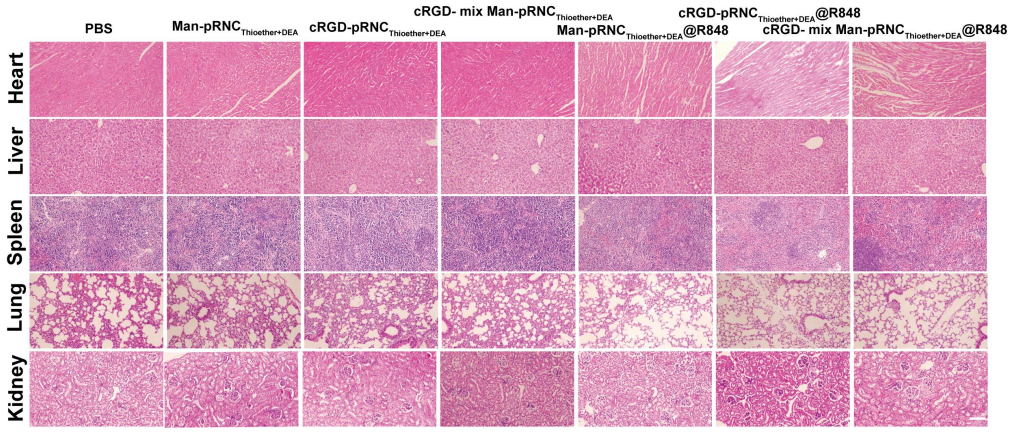

Supplementary Fig. 54. H&E staining of normal tissues harvested from mice in different groups. Scale bar = 100 μm.

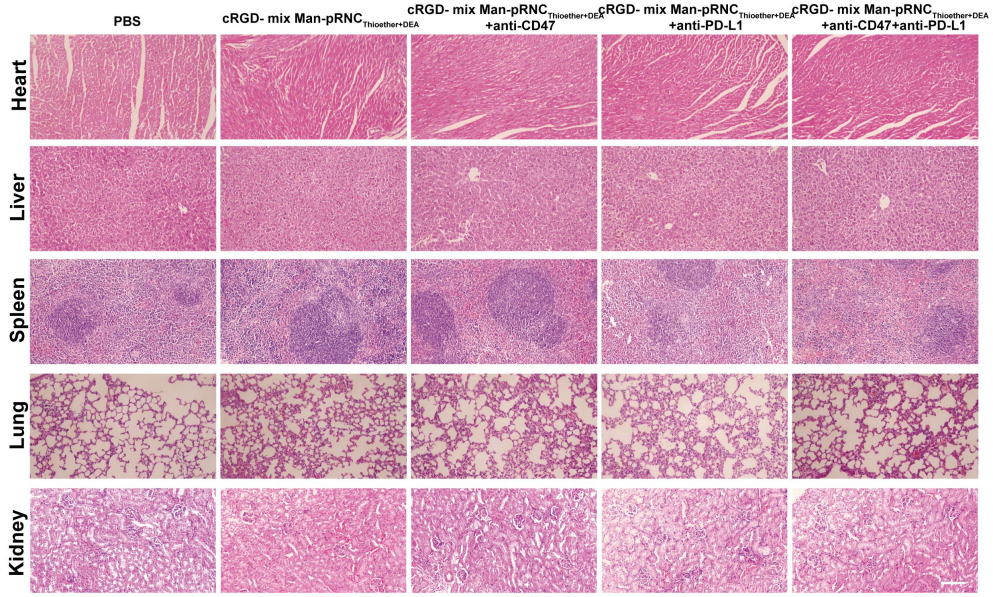

Supplementary Fig. 55. H&E staining of normal tissues harvested from mice in different groups. Scale bar = 100 μm.

Supplementary Table 1. Characteristics of block copolymers.

Copolymers	M_n (kg/mol)		GPC	
	Design	^{1}H NMRa	M_n b (kg/mol)	M_w/M_n b
PEG-PMMA	5.0-12.0	5.0-10.0	15.3	1.30
PEG-PMMA-PPPMA	5.0-12.0-3.0	5.0-10.0-6.3	18.9	1.39
PEG-PMMA-PDEA	5.0-12.0-4.6	5.0-10.0-3.8	19.2	1.35
PEG-PMMA-P(PPMA-ME)	5.0-12.0-9.3	5.0-10.0-10.4	30.7	1.14
PEG-PMMA-P(PPMA-MPA-DEA)	5.0-12.0-16.5	5.0-7.3-18.4	36.1	1.41

[a] Calculated from ^{1}H NMR by comparing the intensities of signals at δ 3.65, 3.60, 2.97, 1.82,

1.24 and 0.82, respectively.

[b] Analyzed by GPC using THF as an eluent at a flow rate of 1.0 mL/min (standards: PMMA, 30 ℃).

Supplementary Table 2. Preparation of blank polymersomes.

Polymersomes	Size (nm)[a]	PDI[a]
NC_{MMA}	118.2 ± 1.5	0.24 ± 0.006
NC_{yne}	138.7 ± 8.2	0.25 ± 0.032
$pRNC_{DEA}$	126.5 ± 3.6	0.22 ± 0.013
$NC_{Thioether}$	132.8 ± 5.6	0.22 ± 0.025
$pRNC_{Thioether+DEA}$	140.7 ± 3.5	0.29 ± 0.010

[a] Determined by Malvern Panalytical Zetasizer Pro at 25 ℃ in PBS (10 mM, pH 7.4).

Supplementary Table 3. Drug loading content and efficiency characterization.

Polymersomes	Thero. DLC (wt.%)	Size[a] (nm)	PDI[a]	DLC[b] (wt.%)	DLE[b] (%)
cRGD-$NP_{Thioether+DEA}$@R848	5%	168.0 ± 4.8	0.22 ± 0.02	4.79	95.6
	10%	236.4 ± 2.5	0.12 ± 0.10	8.28	81.3
	20%	246.5 ± 5.9	0.18 ± 0.02	12.70	58.2
Man-$NP_{Thioether+DEA}$@R848	5%	143.3 ± 5.5	0.16 ± 0.01	4.85	96.8
	10%	143.5 ± 1.0	0.17 ± 0.01	8.46	83.2
	20%	171.4 ± 4.0	0.06 ± 0.02	13.29	61.3
cRGD- *mix* Man-$pRNC_{Thioether+DEA}$@R848	5%	169.9 ± 22.7	0.21 ± 0.06	4.65	92.6
	10%	183.3 ± 4.6	0.16 ± 0.04	8.15	79.9
	20%	176.2 ± 3.9	0.28 ± 0.03	12.55	57.4

[a] Determined using Malvern Panalytical Zetasizer Pro at 25 ℃ in PBS (10 mM, pH 7.4).

[b] Determined by fluorescence spectrophotometer measurement.